Catalysis Today 147S (2009) S2–S9

Contents lists available at ScienceDirect

Catalysis Today

journal homepage: www.elsevier.com/locate/cattod

Experimental and numerical comparison of structured packings with a randomly packed bed reactor for Fischer–Tropsch synthesis

Kalyani Pangarkar [a,c,*], Tilman J. Schildhauer [b], J. Ruud van Ommen [c], John Nijenhuis [c], Jacob A. Moulijn [a], Freek Kapteijn [a,**]

[a] Catalysis Engineering, Delft University of Technology, Julianalaan 136, 2628 BL Delft, The Netherlands
[b] Laboratory for Energy and Materials Cycles, Paul ScherrerInstitut, 5232 Villigen PSI, Switzerland
[c] Product and Process Engineering, Delft University of Technology, Julianalaan 136, 2628 BL Delft, The Netherlands

ARTICLE INFO

Keywords:
Radial heat transport
Multitubular fixed bed reactor
Fischer–Tropsch synthesis
Structured packings
Reactor modeling

ABSTRACT

The potential of four structured packings has been explored for application in highly exothermic multiphase reactions such as the Fischer–Tropsch synthesis where removal of reaction heat is a major issue in the packed bed reactor type. Efficient heat removal is extremely critical to keep the catalytic activity and selectivity in the desired range. Structured internals can play a very important role in improving heat transport and allow solutions that were previously impossible. The catalyst size and shape can be tailored such that an optimal combination of reaction kinetics, pressure drop and heat transfer characteristics is obtained.

A dedicated set-up was designed and built to measure the radial heat transport in two-phase flow at ambient pressure in the absence of reaction. The structured packings – especially open and closed cross flow structures (OCFS and CCFS) – exhibit radial heat transport superior over that of packed bed of glass beads, and at lower energy dissipation. A 2D reactor model for Fischer–Tropsch synthesis, based on heat and mass balances including gas–liquid, liquid–solid and intraparticle diffusion transport, is used to compare the performance of a tubular fixed bed reactor either packed with spherical particles or equipped with the OCFS packing. The simulations indicate that a reactor with a structured packing can be operated with at least twice the reactor diameter compared to the packed bed reactor without any significant loss in the STY. A structured bed reactor can considerably contribute to process intensification.

1. Introduction

Structured packings such as open cross flow structures (OCFS), closed cross flow structures (CCFS), foams and knitted wire (Fig. 1) as catalyst supports have certain advantages over randomly packed beds due to their well-defined geometry [1]. OCFS and foams are well-known for their excellent radial mixing properties. Similarly, CCFS are expected to have good radial heat transport as flow in these structures is directed in radial direction towards the wall. Knitted wire is well-known for its high mass transfer efficiency in distillation [2].

So far, almost no research effort has been put in heat transfer studies in structured packings for two-phase flow as they are hardly used in applications where heat transfer is a major issue. Some work has already been published regarding heat transfer measurements in single gas phase flow, namely for Katapak-M catalyst supports [3], ceramic foam catalyst supports [4], honeycomb monoliths [5], OCFS packings [6] and CCFS packings [7].

In this work, we have investigated the radial heat transport in terms of the effective radial thermal conductivity, $\lambda_{e,r}$, and wall heat transfer coefficient, α_w of the four structured packing types mentioned above with co-current gas–liquid flow, and compared this with the performance of a packed bed of glass beads. A reactor model for Fischer–Tropsch synthesis is developed for a single tube equipped with these packings to explore if the improved radial heat transport properties of the structured packing allow the use of more active catalysts or of larger reactor diameters without loss of selectivity or productivity.

2. Experimental

2.1. Structured packings

In this study, we have investigated four different structure packings (see Fig. 1).

* Corresponding author at: Catalysis Engineering, Delft University of Technology, Julianalaan 136, 2628 BL Delft, The Netherlands.
** Corresponding author.
E-mail addresses: kalyanimv@hotmail.com (K. Pangarkar), f.kapteijn@tudelft.nl (F. Kapteijn).

0920-5861/$ – see front matter © 2009 Elsevier B.V. All rights reserved.
doi:10.1016/j.cattod.2009.07.035

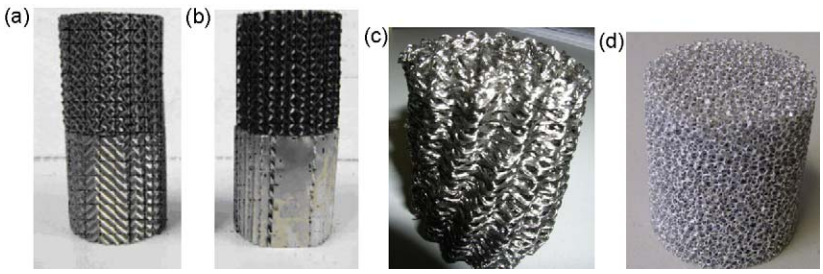

Fig. 1. Structured packings used: (a) OCFS, (b) CCFS, (c) knitted wire and (d) aluminum foam.

The *OCFS structure* consists of superimposed individual corrugated metal sheets, with the corrugations in opposed orientation for neighbouring plates [3]. The radial convection in these structures is a part of mixing flow patterns between adjacent corrugated sheets.

The *CCFS structure* is derived from that of OCFS by inserting flat sheets between adjacent corrugated sheets. The flow in these structures is directed in radial direction without any mixing of adjacent flow paths, except in the gap between the structure and the reactor wall [7]. Inside the structure, heat is transferred by conduction only through the corrugated walls.

The *knitted wire packing* is characterized by bundles of knitted strands of stainless steel wires which are flattened, crimped and rolled to give the desired diameter of the packing. The crimps run either from top left to bottom right or *vice versa*, promoting fluid remixing at the changeover points [2]. The capillary nature of the filaments helps in spreading the liquid over the complete cross-section.

Foam materials consist of small ligaments that are continuously connected in an open-celled Al-foam structure. A radial orientation of the cells is desired for convective heat transport in the radial direction. The tortuous flow paths through the porous matrix promote turbulence and increase convective heat transfer [4].

The structured packings, particularly the cross flow structures and foams are anisotropic: they do not possess the same properties in different radial directions. Therefore the heat transport will be different, resulting in different temperature profiles along different angular positions at the same axial position. Table 1 provides the properties of the structured packings and the glass beads that are used as a reference material in this study.

Table 1
Properties of packings used in the experimental study.

Packing	Material	ε	d_h (mm)	a_v (m^{-1})
Glass beads	Silica	0.4	0.9	2000
Open cross flow	Stainless steel	0.84	1.8	1885
Closed cross flow	Stainless steel	0.95	1.6	2400
Knitted wire	Stainless steel	0.9	1.9	1932
Foam	Aluminum	0.9	2.4	1800–2000

2.2. Experimental set-up

Heat transfer experiments were carried out in a set-up using the constant wall temperature approach. The radial and axial temperature profiles were measured as generated by cooling a heated mixture of Isopar-M (organic liquid consisting of C_{13}–C_{16} isoparaffins) and nitrogen flowing co-currently downwards in a 60 cm long, 5 cm I.D. "heat transfer" column (Fig. 2).

The radial temperature profiles are measured by 84 K-type thermocouples at three different angular positions and four different axial positions. The heat transferred from the packing in the column to the cooling water is determined from radial and axial temperature profiles. For the determination of the heat transfer properties, the three radial profiles at different angular positions were averaged [8]. The cooling obtained in the column depends mainly on the packing used and the gas and liquid flow rates.

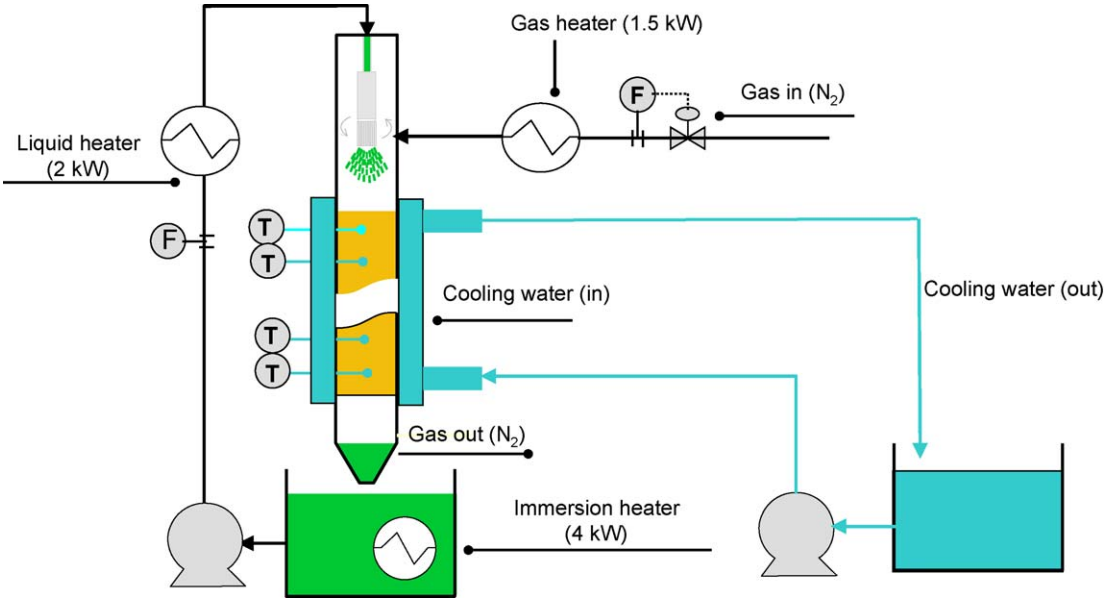

Fig. 2. Schematic diagram of the heat transfer set-up.

3. Experimental results

The heat transfer performance of the packings are compared based on three parameters presented in Fig. 3, *viz.* the effective radial thermal conductivity, $\lambda_{e,r}$, wall heat transfer coefficient, α_w and overall heat transfer coefficient, U_{ov}. The former two parameters were estimated from a steady state heat balance for a two-dimensional pseudo-homogeneous plug flow reactor model, while the latter was calculated from the overall decrease in 'mixing-cup' temperature of the liquid. The two-dimensional energy balance reads:

$$\underbrace{(u_L C_{pL}\rho_L + u_G C_{pG}\rho_G)\frac{\partial T}{\partial z}}_{\text{Axial transport of heat}} = \underbrace{\lambda_{e,r}\left[\frac{\partial^2 T}{\partial r^2} + \frac{1}{r}\frac{\partial T}{\partial r}\right]}_{\text{Radial transport of heat}} \quad (1)$$

The following boundary conditions apply

$$\text{At} z = 0 \quad T = T_{in} \quad (2)$$

$$\text{At} r = 0 \quad \frac{\partial T}{\partial r} = 0 \quad (3)$$

$$\text{At} r = R \quad -\lambda_{eff}\frac{\partial T}{\partial r} = \alpha_w (T_{r=R} - T_w) \quad (4)$$

Eq. (1) is solved using the method of lines with Athena Visual Studio© to fit the computed temperature profiles inside the packing to the experimental ones and optimizing the values of the two parameters $\lambda_{e,r}$ and α_w by non-linear least squares minimization of the difference between computed and experimental temperatures.

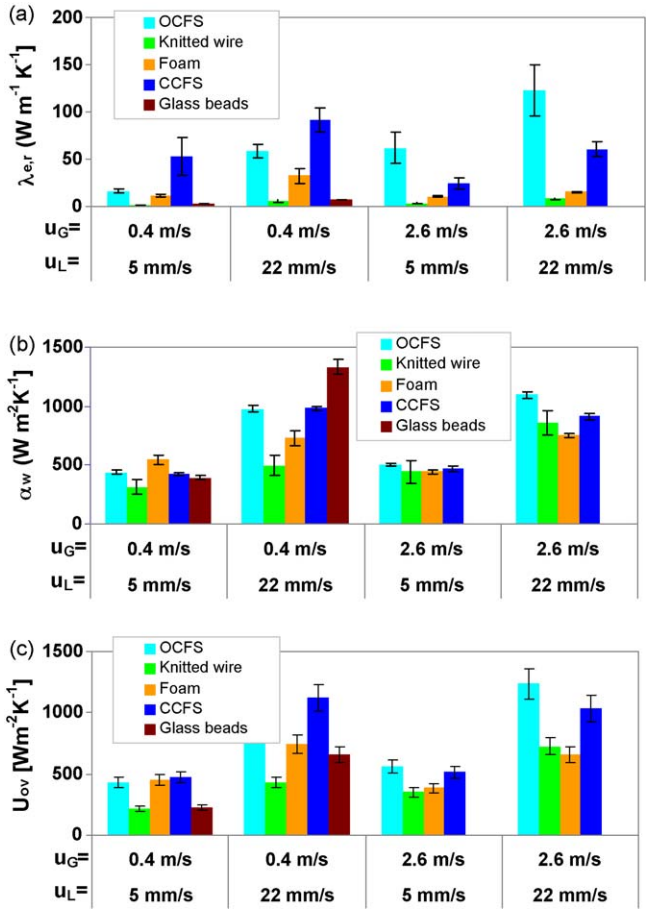

Fig. 3. Estimated values of (a) effective radial conductivity $\lambda_{e,r}$, (b) wall heat transfer coefficient α_w and (c) overall heat transfer coefficient, U_{ov} for the various packings at four different flow conditions.

The low $\lambda_{e,r}$ values for foam and knitted wire in Fig. 3a indicate that in these packings mainly conductive heat transport takes place, with a virtually absent convective component. The high $\lambda_{e,r}$ values in CCFS and OCFS, up to 100 W/K/m, indicate that the radial transport is not the limiting factor for the heat transfer process, and fairly flat radial temperature profiles can be obtained. This confirms their anticipated excellent radial transport properties.

The values for α_w at low liquid velocities are roughly the same for all packings, ranging from 300 to 1000 W/K/m^2 (Fig. 3b). At low liquid velocities, the convective flow of liquid near the wall is not significant and conductive transport of heat plays a dominant role. At high liquid velocities differences between the packings are more prominent. The glass beads perform better at high liquid velocities due to the higher convective flow rate at the wall leading to the formation of liquid eddies with effective heat transfer. The convective flow of liquid is less significant in the structured packings, resulting in lower α_w at the same liquid and gas velocities.

The radial orientation of the convective flow in CCFS and OCFS yields higher values of α_w (up to 1200 W/m^2/K) than for the foam and knitted wire, but lower than for glass beads.

As an overall result, the overall heat transfer coefficient U_{ov} (Fig. 3c) is about two times larger for OCFS and CCFS than for glass beads. For the cross flow structures the main resistance to heat transfer is near the wall, *i.e.* α_w determines the total heat transfer rate. Cross flow geometries clearly have an increased heat transfer performance, which is not captured by the two-dimensional pseudo-homogeneous plug flow model as this model does not take directed convective transport of heat into account [9].

Note that the axial thermal conductivity is neglected in estimating the parameters. This assumption may not entirely hold for the foam packing due to the conductive properties of the aluminum matrix. The $\lambda_{e,r}$ and α_w values obtained at low flow rates are perhaps lower than the true values due to the presence of axial conduction. This probably does not hold for OCFS and CCFS structures due to their excellent radial mixing properties thus resulting in a more uniform velocity profiles and plug flow behaviour. Moreover the conduction through the 90% porous steel structure is minimal if compared to the aluminum foam structure.

4. Reactor modeling

A model-based quantitative comparison is made between the performance of two fixed bed FTS reactors; one filled with spherical catalyst particles and the other equipped with a structured packing. The OCFS is chosen as the desired structured packing because of its reasonably good mass transfer [10] and excellent heat transport characteristics as compared to the other structured packings, and its commercial availability. Table 2 gives the geometry details for the particles and OCFS used in the modeling study, considering a base case reactor diameter of 5 cm and length of 20 m. Full details are given elsewhere [11].

Table 2
Geometric parameters of packings used in simulation.

Parameter	Packed bed with spheres	Structured bed with OCFS	Structured bed with OCFS
Metal hold-up, ε_m	–	0.05	0.05
Catalyst dimension (mm)	d_p = 2.2	L_c = 0.085	L_c = 0.085
Specific surface area, a_v ($m^2_{catalyst}/m^3_{reactor}$)	1640	2000	4000
Catalyst hold-up, ε_{cat}	0.6	0.17	0.34
Bed porosity, ε	0.4	0.78	0.61
External surface area, a_p ($m^2_{catalyst}/m^3_{catalyst}$)	2730	11,760	11,760

The Fischer–Tropsch synthesis is chosen for the comparison between the two multiphase fixed bed reactors, as a demanding reaction where heat and mass transport issues are strongly intertwined, determining the overall reactor performance. In FTS synthesis gas is converted into liquid fuels. Typical operating conditions are pressures between 10 and 60 bar and temperatures in the range of 200–350 °C [12,13]. FTS follows a polymerization mechanism in which hydrocarbon products such as n-paraffins and olefins ranging from methane to heavy waxes are produced. A high chain growth probability resulting in a high selectivity to the middle distillates and waxes (C_{5+} products) is favoured by a proper selection of catalyst properties, temperature and reactant pressure and composition. The typical characteristics of the low temperature (200–250 °C) FT process important for any reactor type are:

1. The selectivity to the desired C_{5+} products is a strong function of the reaction temperature, decreasing with increasing temperature and increasing H_2/CO ratio.
2. The FTS process is highly exothermal with a heat of reaction of ~167 kJ/mol, causing temperature gradients in axial and radial reactor direction. The large amount of heat released puts constraints on the reaction temperature in view of the selectivity.
3. Mass transport limitations are important as well, as they may reduce the productivity and selectivity to C_{5+} FT products. Although the reactants are in the gas phase, the pores of the catalyst are filled with liquid products. The diffusion in the liquid phase is typically three orders of magnitude slower than in the gas phase, and, as a consequence, the FTS may be intraparticle diffusion limited. Increasing severity of transport limitations (due to higher reaction rates or longer diffusion distances) will eventually result in faster depletion of the slower diffusing CO, resulting in very high H_2/CO ratios inside the catalyst pellet, leading to enhanced methanation and lower selectivities to C_{5+}.
4. Low gas to liquid mass transfer rate may affect the liquid phase concentrations of the reactants, lowering the productivity.

In this perspective, the reactor types used commercially at the moment are compromises.

The steady state reactor model developed is based on convective flow through packed bed reactors filled with either particles or a structured packing. Axial dispersion is neglected, based on the superior radial mixing properties of OCFS and the fairly low dispersion in the random bed reactor, and validated with existing correlations given for structured packings. No radial dispersion of momentum and mass was considered, *i.e.* velocity and concentration gradients were assumed to be absent in the radial direction.

The major transport phenomena included in this model are (i) convective transport of gas and liquid, (ii) gas to liquid mass transfer, (iii) liquid to solid mass transfer, (iv) intraparticle diffusion in pellets and coatings, (v) convective axial and radial heat transport, and (vi) pressure drop. Most importantly a selectivity model is used based on the chain growth probability parameter α in the Anderson–Schulz–Flory model, which varies as a function of temperature and H_2/CO ratio instead of being constant as commonly used for a Co catalyst. The chain growth probability evolves to the proper limits for changing H_2/CO ratio and temperature. Experimental data for a Co/γ-Al_2O_3 catalyst from de Deugd [14] and Co–ZrO_2 from Patzlaff et al. [15] have been used to estimate the two parameters in the α-model.

$$\alpha = \frac{1}{1 + k_0 \exp(-\Delta E/RT)(C_{s,H_2}/C_{s,CO})^{0.5}} \tag{5}$$

with k_0 = 22.1 and ΔE = 19,822 J/mol.

The CO conversion is based on the rate expression given by Yates and Satterfield [16] for a Co/MgO catalyst. The temperature dependency of the parameters in the rate expression has been determined by Maretto and Krishna [17] from the data of Yates and Satterfield.

$$r_{syngas} = \frac{a\, p_{H_2}\, p_{CO}}{(1 + b\, p_{CO})^2} \tag{6}$$

$$a = 8.8533 \times 10^{-3}\left[4494.41\left(\frac{1}{493.15} - \frac{1}{T}\right)\right] \tag{7}$$

$$b = 2.226 \exp\left[-8236\left(\frac{1}{493.15} - \frac{1}{T}\right)\right] \tag{8}$$

In total eight components are considered for the molar balances namely: H_2, CO, H_2O, C_1, C_2, C_3, C_4 and C_{5+}. In axial direction molar balances are defined for reactants CO and H_2, and products water and hydrocarbons up to C_4, for both the gas and liquid phase. The products higher than C_4 are lumped as C_{5+} and are assumed to be completely in the liquid phase. The molar gas flow rate is modeled as a variable, because the FTS reaction causes a strong contraction of the gas phase of about 65% at full conversion resulting in a significant decrease in the gas volume. The liquid flow rate is also allowed to change along the length of the reactor as the amount of hydrocarbons formed by reaction is of the order of the liquid recycle stream fed to the reactor. Changes in liquid density are neglected as it is not a strong function of temperature. A liquid phase heat balance is used to describe the temperature profile along the reactor length (axial) and in radial direction. The physical properties such as liquid heat capacity and liquid density are taken from Marano and Holder [18] assuming the wax consists of n-paraffin with carbon number 28 ($C_{28}H_{58}$). The correlations to estimate the solubility of reactant and product gases in the liquid wax have been taken from Marano and Holder [19].

The transport of reactants and products through the catalyst pores filled with a liquid phase is described by Fickian diffusion. The liquid phase diffusivities have been estimated from Wang et al. [20]. The corresponding effective diffusivity of component *i* in the catalyst pores is calculated by correcting the molecular diffusivity with the porosity and tortuosity [21].

The individual local production and depletion rates r_i of the reactants and products are calculated based on the Yates and Satterfield kinetic expression and the ASF chain growth probability α at each position within the catalyst and in the reactor. The C_{5+} production is normalised with respect to C_{28} and is taken as the sum of the production of C_{5+} until C_{200}.

$$r_{H_2} = -2r_{syngas} \quad r_{CO} = -r_{syngas} \quad r_{H_2O} = r_{syngas} \tag{9}$$

$$r_{C_1} = (1-\alpha) r_{syngas} \tag{10}$$

$$r_{C_2} = (1-\alpha)\alpha r_{syngas} \tag{11}$$

$$r_{C_3} = (1-\alpha)\alpha^2 r_{syngas} \tag{12}$$

$$r_{C_4} = (1-\alpha)\alpha^3 r_{syngas} \tag{13}$$

$$r_{C_{5+}} = \sum_{n=5}^{n=200} (1-\alpha)\alpha^{n-1} r_{syngas} \tag{14}$$

An average α is estimated for each pellet/coating at each location in the reactor from the production of methane,

$$\frac{r_{CH_4}}{r_{syngas}} = (1 - \alpha_{average}) \tag{15}$$

The effective CO consumption rate inside the particle which includes the effect of internal diffusion limitations required to

calculate the average rate of heat production in the energy balance, is calculated from the boundary condition at the catalyst surface:

$$k_{LS}a_p(C_{co,L} - C_{co,S}) = D_{co,eff}\frac{2}{d_p}\frac{\partial C_{co,cat}}{\partial \xi}\bigg|_{\xi=1} \quad a_p = r_{eff,co}\rho_{pellet} \qquad (16)$$

Two models of increasing complexity are considered to study the effect of radial temperature gradients on space time yield, STY, and selectivity for C_{5+}.

4.1. 1D reactor model

A simplified energy balance has been used, assuming that the temperature at any axial position is the same at all radial positions. This assumption is valid when the radial transport of heat is efficient, so when $\lambda_{e,r}$ is high, giving rise to nearly flat temperature profiles, like in the cross flow structures, and only a wall heat transfer process is considered.

4.2. 2D reactor model

A pseudo-homogeneous tubular reactor model with axial and radial temperature gradients, simulated using the effective radial heat conductivity $\lambda_{e,r}$ and the wall heat transfer coefficient α_w. When $\lambda_{e,r}$ is small, steep temperature gradients are produced in the radial direction of the packed bed. For an exothermal reaction such as the Fischer–Tropsch synthesis, taking place inside the catalyst bed, the temperature at the centre of the tube will be the highest and the temperature at the wall of the tube will be the lowest. This gives rise to different effective reaction rates at local radial positions, which in turn affects the selectivity and productivity of the catalyst and reactor. This model was used to compare the random packed bed reactor with the structured reactor so that the effect of temperature deviations on the STY and selectivity can be highlighted.

The steady state models are solved as an initial value problem for the 1D model and an initial boundary value problem (IBVP) for the 2D model in Athena Visual Studio [22].

5. Simulation results

5.1. Catalyst activity

The performance of the packed bed is compared with that of OCFS2000 and OCFS4000 (OCFS with a specific surface area to 2000 and 4000 m^{-1}, respectively) at different catalyst activities in terms of the Yates and Satterfield (YS) kinetics in Fig. 4 using the 1D reactor model. Nearly in all cases the packed bed is the poorest reactor except for the low rates where the packed bed performs better than OCFS2000 due to its higher catalyst inventory. At these low rates OSCF4000 performs the best with respect to both selectivity and productivity. At very high reaction rates (10*YS), both OCFS4000 and OCFS2000 perform better than the packed bed. The STY (space time yield) to C_{5+} obtained at 5YS is higher than at 10YS for all packings (Fig. 4c). Though the activity at 10YS is higher than at 5YS (Fig. 4a), the selectivity to C_{5+} decreases with increasing reaction rate and hence is lower at 10YS than at 5YS (Fig. 4b). The loss in selectivity with increasing catalytic activity is mainly due to increasing intraparticle diffusion problems as follows from Fig. 5. It is emphasized that the reaction conditions differ, *i.e.* the gas hourly space velocity, GHSV, chosen for 1YS (27 $m^3_{gas}/m^3_{reactor}/h$) is lower than that used for 5YS and 10YS (137 $m^3_{gas}/m^3_{reactor}/h$), in order to keep the CO conversion above 50%.

Thus the conversion obtained at 1YS cannot be directly compared to that obtained at 5YS and 10YS in Fig. 4a.

Fig. 5 compares the intraparticle diffusion limitations for the packed bed and OCFS2000 when the rate is increased from 1YS to 10YS. The internal concentration profiles of hydrogen and CO get steeper at higher reaction rates, indicating increasing internal diffusion limitations for both packings. Also apparent is the slower diffusion of CO. CO becomes depleted in the particle interior, unlike hydrogen, and this effect is more pronounced for the particulate catalyst. The extent of internal diffusion limitation results in different selectivity to C_{5+} for the different reactor types as seen in Fig. 4b, attributed to the strongly increasing H_2/CO ratio. Thus the OCFS2000 with the least diffusion limitations shows the highest selectivity values, but closely followed by OCFS4000. The latter has in all cases the highest C_{5+} yield. This is attributed to its larger catalyst inventory, while the catalyst layer thickness is kept the same. Increasing the catalyst activity from 5YS to 10YS does not further improve the reactor yields for all packings, due to the strong intraparticle diffusion limitations (Fig. 5).

So, with increasing catalytic activity, the performance of the packed bed worsens as compared to the structured packings due to strong diffusion limitations.

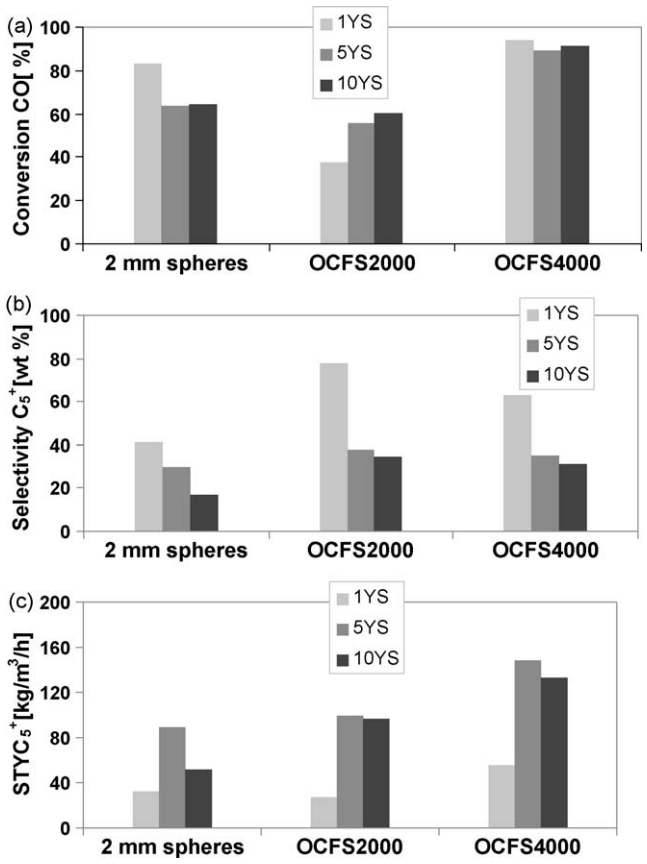

Fig. 4. Comparison between packed bed of spheres, OCFS2000 and OCFS4000 using the 1D reactor model for three catalyst activity levels r_{syngas} = 1YS, 5YS and 10YS. (a) CO conversion; (b) selectivity to C_{5+}; (c) STY to C_{5+}. Reaction conditions: T_{in} = 490 K, $T_{coolant}$ = 490 K, u_G = 0.15 m/s, u_L = 0.01 m/s at r_{syngas} = 1YS and u_G = 0.76 m/s, u_L = 0.02 m/s at r_{syngas} = 5YS and 10YS. H_2/CO feed ratio = 2.0.

5.2. Radial reactor temperature profiles—reactor diameter sensitivity

An important practical aspect of multitubular reactors is the number of reactor tubes. Reducing the number of tubes by increasing the diameter and maintaining the productivity is attractive and results in lower investment. The reactor diameter can be increased only if the increasing radial temperature gradients do not lower the selectivity and STY to the desired products. Therefore, a sensitivity analysis has been performed

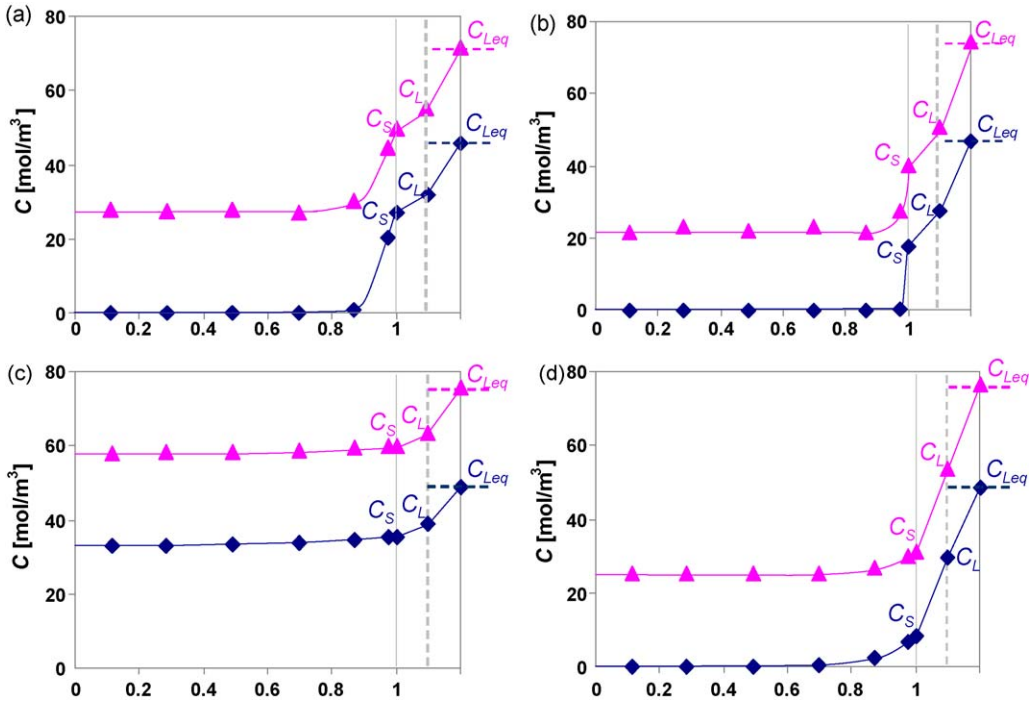

Fig. 5. H_2 (▲) and CO (◆) liquid phase concentration profiles at z = 0.1 from the gas–liquid interface, C_{Leq}, bulk liquid concentration, C_L, surface concentration, C_S, to the catalyst interior (1 = catalyst surface, 0 = centre) for r_{syngas} = 1YS (left) and (b) r_{syngas} = 10YS (right). Packed bed with 2 mm spheres (a and b) and OCFS2000 (c and d). Further conditions as in Fig. 4. (For interpretation of the references to color in this figure legend, the reader is referred to the web version of the article.)

relative to the base case diameter, using the 2D reactor model for both packings, with respect to the selectivity or and STY to C_{5+}.

In case of the structured packing, the high $\lambda_{e,r}$ values result in flatter temperature profiles and hence at increasing reactor diameter the loss of selectivity is much smaller than for the packed bed. In this particular case (Fig. 6a), the C_{5+} STY only shows a minor decrease when doubling the base case reactor diameter ($2d_{tube}$). This is a major advantage to the process as eventually a

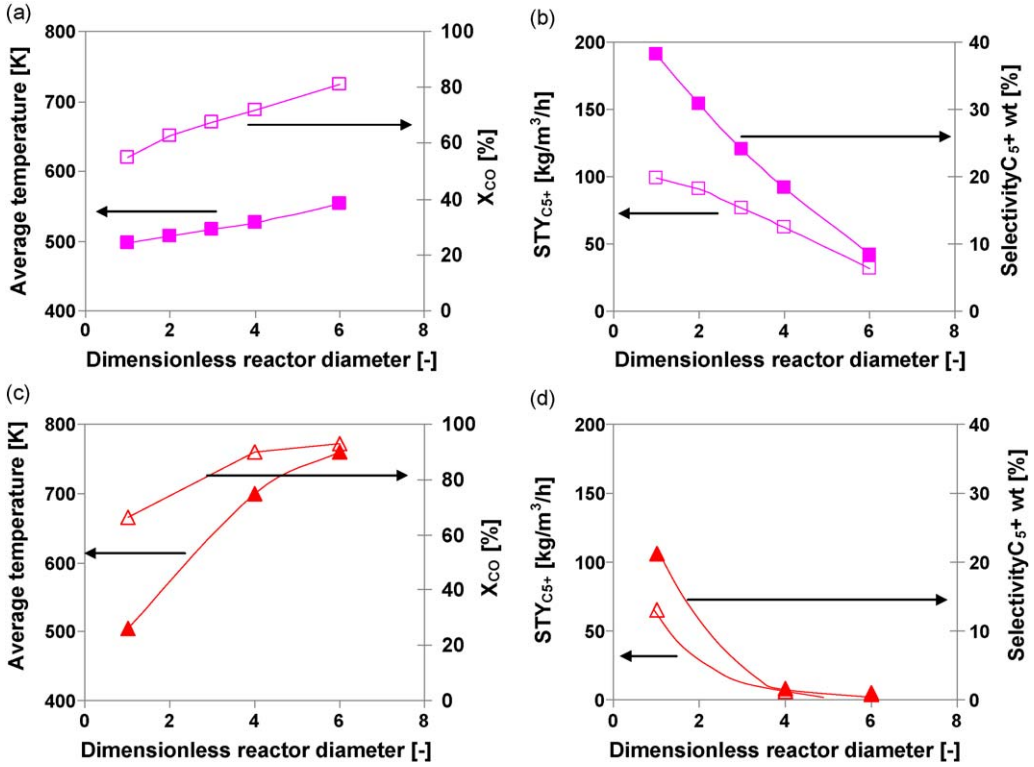

Fig. 6. 2D modeling results for increasing reactor diameter for OCFS2000 (top) and 2 mm spheres packing (bottom): (a and c) □ △ CO conversion and ■ ▲ average temperature and (b and d) □ △ STY to C_{5+} and ■ ▲ wt% selectivity to C_{5+}. Reaction conditions: T_{in} = 490 K, $T_{coolant}$ = 490 K, u_G = 0.76 m/s, u_L = 0.02 m/s, H_2/CO feed ratio = 2.0, r_{syngas} = 5YS. (For interpretation of the references to color in this figure legend, the reader is referred to the web version of the article.)

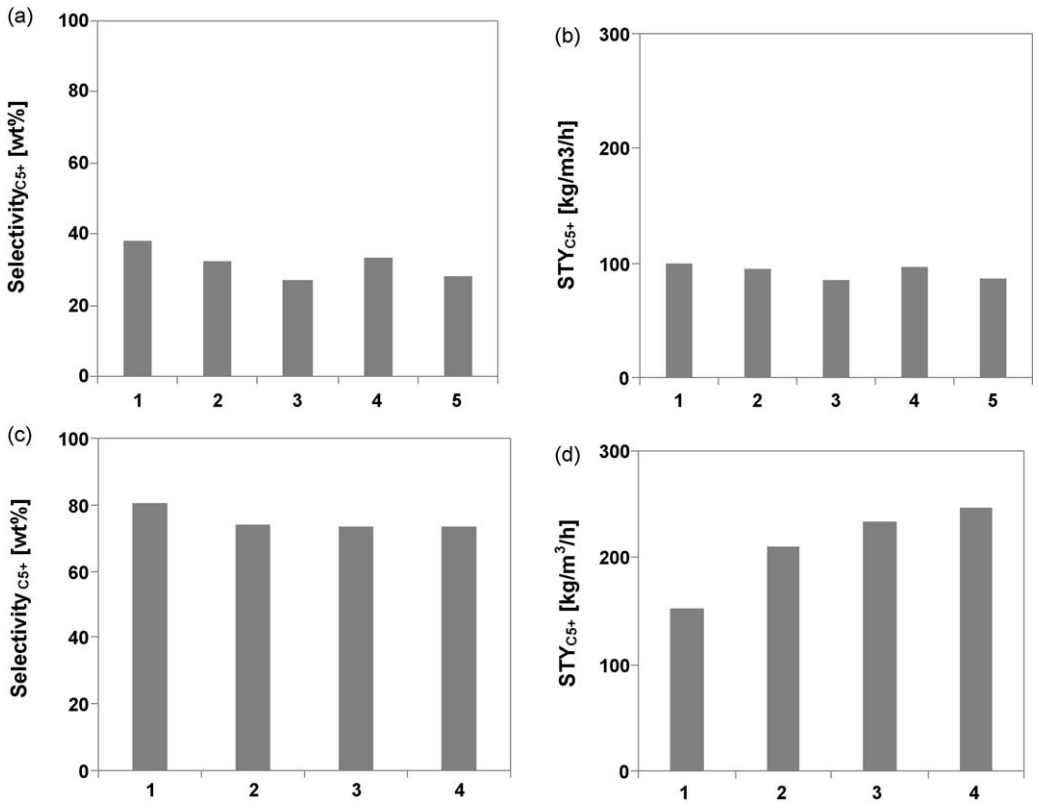

Fig. 7. Influence of wall heat transfer coefficient and temperature for OCFS2000 on (a and c) selectivity to C_{5+} (wt%) and (b and d) STY to C_{5+} for H_2/CO feed ratio = 2.0 (top) and 1.5 (bottom). Key, 1:α_w = 1075 W/(m^2 K), T_{in} = 490 K; 2: α_w = 2000 W/(m^2 K), T_{in} = 505 K; 3: α_w = 2000 W/(m^2 K), T_{in} = 515 K; 4: α_w = 3000 W/(m^2 K), T_{in} = 505 K (a and b), 4: α_w = 3000 W/(m^2 K), T_{in} = 525 K (c and d), 5: α_w = 3000 W/(m^2 K), T_{in} = 515 K. Results obtained for 1D model. Reaction conditions: u_G = 0.76 m/s, u_L = 0.02 m/s, r_{syngas} = 5YS, T_{in} = $T_{coolant}$ in all simulations.

smaller number of reactor tubes can be used while maintaining the productivity. In case of the packed bed reactor the increase in reactor diameter has a very negative impact on the selectivity and STY (Fig. 6b). Generally an increase in reactor diameter results in higher temperature levels in the centre of the reactor. Although it leads to higher reaction rates, due to higher temperature levels selectivity and STY decrease considerably.

5.3. Variation wall heat transfer coefficient and inlet temperature

Further increase of the reactor diameter decreases the heat exchange area to volume ratio having a negative impact on the heat removal of the reactor and an optimum in diameter is expected for given heat transport parameters.

So, as heat conduction for the structured packing is very good, improvement of the wall heat transfer could be a next objective. At higher α_w higher temperature levels can be afforded inside the reactor without a large penalty on selectivities. This can be achieved by increasing the inlet temperature at increasing α_w. The results are disappointing: a combination of larger α_w together with higher inlet temperature does not lead to a higher STY (Fig. 7a and b). We anticipated a higher sensitivity for conditions of high selectivity.

Therefore we carried out simulations at a H_2/CO ratio of 1.5 that give higher selectivity to C_{5+} products, >80% (Fig. 7c). At these process conditions an improved α_w in combination with higher inlet temperature does boost the STY. Thus increasing α_w by two times and the reactor inlet temperature from 490 to 525 K brings about a quite significant 60% increase in STY (Fig. 7d).

The influence of α_w on the performance of the reactor, e.g. STY, is thus a function of various process parameters. In this particular case for the chosen selectivity model, the influence is largely dominated by the H_2/CO feed ratio.

The results presented above show that increasing the catalyst activity only will not help getting the best out of a fixed bed reactor type. Thus the ultimate goal should be to aim for a multiphase contactor which is not limited in any of the above transport processes and gives an opportunity to exploit the increased catalyst activity and selectivity to the fullest.

The results demonstrate the good opportunities for the application of structured packings in gas–liquid–solid reactors to remove or supply energy. The excellent radial heat transport allows the use of larger reactor diameters and/or more active catalysts in fixed bed reactors for multiphase operation. This may reduce the number of reactor tubes in multitubular reactors.

6. Conclusions

In this work, we have determined the following heat transfer parameters: effective radial thermal conductivity, $\lambda_{e,r}$, wall heat transfer coefficient, α_w using a two-dimensional pseudo-homogeneous plug flow model and overall heat transfer coefficient, U_{ov} for a gas–organic liquid system flowing in a co-current down-flow mode in four structured packings, and used these to evaluate the performance of their application as a catalyst support in a Fischer–Tropsch process. The radial heat transport in structured packings in gas–liquid co-current down-flow mode is far better than of randomly packed beds. Important conclusions from this work are:

- The overall heat transfer coefficient U_{ov} of both closed cross flow structures (CCFS) and open cross flow structures (OCFS) is higher than foam and knitted wire mesh. Their U_{ov} value is two times higher than that of glass beads packing.
- Due to radial heat transport limitations and very strong internal diffusion limitations, the random packed bed reactor is more

sensitive to inlet temperatures than a structured bed. This allows the latter to operate at higher reactor inlet temperatures since the C_{5+} selectivity is maintained by the improved heat transfer.
- For the same reason a packed bed cannot be operated at larger reactor diameters, whereas a structured packing can be operated with at least twice the reactor diameter without any significant loss in the STY for C_{5+}.
- An increase in α_w in combination with a higher reactor inlet temperature results in a higher STY of C_{5+} only at H_2/CO inlet ratios below 2. At higher ratios the process is relatively insensitive to improvements in the wall heat transfer rates.

In conclusion, this study of the application of a structured catalyst in a FTS reactor has revealed clear advantages of the improved radial heat transport properties, allowing the application of more active catalysts and the use of larger reactor diameters. It gives an outlook for process intensification in fixed bed FTS reactors.

Notations

a	kinetic constant of the Yates and Satterfield rate (mol/(s kg_{cat} bar^2))
a_p	external catalyst surface area ($m^2_{catalyst}/m^3_{catalyst}$)
a_v	geometric surface area of the packing ($m^2_{catalyst}/m^3_{reactor}$)
b	adsorption constant of the Yates and Satterfield rate (1/bar)
C_L	liquid phase concentration (mol/m^3)
$C_{L,eq}$	equilibrium concentration (mol/m^3)
C_{pL}	liquid heat capacity (J/kg/K)
C_{pG}	liquid heat capacity (J/kg/K)
C_S	concentration at surface of the catalyst (mol/m^3)
d_h	hydraulic diameter (m)
d_p	particle diameter (mm)
D_{eff}	effective diffusivity inside catalyst pores (m^2/s)
k_{LS}	liquid–solid intrinsic mass transfer coefficient (m/s)
k_0	parameter in chain growth probability correlation
L_c	slab thickness (m)
r_{syngas}	intrinsic reaction rate (mol/kg_{cat}/s)
P	pressure
T	temperature (K)
U_{ov}	overall wall heat transfer coefficient (W/m^2 s K)
u_G	superficial gas velocity (m/s)
u_L	superficial liquid velocity (m/s)

Greek letters

α	chain growth probability
α_w	wall heat transfer coefficient (W/(m^2 K))
ΔE	parameter in chain growth probability correlation (J/mol)
$\lambda_{e,r}$	radial effective thermal conductivity (W/(m K))
ε	bed porosity
ε_{cat}	catalyst hold-up
ρ_G	gas density (kg/m^3)
ρ_L	liquid density (kg/m^3)
ρ_{pellet}	catalyst pellet density (kg/m^3)

References

[1] K. Pangarkar, T.J. Schildhauer, J.R. van Ommen, J. Nijenhuis, F. Kapteijn, J.A. Moulijn, Ind. Eng. Chem. Res. 47 (2008) 3720–3751.
[2] L.B. Bragg, Ind. Eng. Chem. 49 (1957) 1062–1066.
[3] C. von Scala, M. Wehrli, G. Gaiser, Chem. Eng. Sci. 54 (1999) 1375–1381.
[4] J.T. Richardson, D. Remue, J.K. Hung, Appl. Catal. A: Gen. 250 (2003) 319–329.
[5] G. Groppi, E. Tronconi, Catal. Today 105 (2005) 297–304.
[6] G. Eigenberger, V. Kottke, T. Daszkowski, G. Gaiser, H.J. Kern, Regelmässige Katalysatorformkörper für technische Synthesen, Fortschritt-Berichte VDI. Reihe 15, Umwelttechnik, Nr. 112.
[7] T.J. Schildhauer, E. Newson, A. Wokaun, Chem. Eng. Process.: Process Intens. 48 (2009) 321–328.
[8] K. Pangarkar, T.J. Schildhauer, J.R. van Ommen, J. Nijenhuis, F. Kapteijn, J.A. Moulijn, Chem. Eng. Sci., in preparation.
[9] D. Vervloet, M.R. Kamali, J.J.J. Gillissen, J. Nijenhuis, H.E.A. van den Akker, F. Kapteijn, J.R. van Ommen, Catal. Today, this issue.
[10] J. Battista, U. Bohm, Chem. Eng. Technol. 26 (2003) 1061–1067.
[11] To be published, 2009.
[12] B. Jager, R.L. Espinoza, Catal. Today 23 (1995) 17–28.
[13] S.T. Sie, Rev. Chem. Eng. 14 (1998) 109.
[14] R.M. de Deugd, Fischer Tropsch synthesis revisited, PhD thesis, Delft University of Technology, Delft, The Netherlands, 2004.
[15] J. Patzlaff, Y. Liu, C. Graffmann, J. Gaube, Catal. Today 71 (2002) 384–391.
[16] I.C. Yates, C.N. Satterfield, Energy Fuels 5 (1991) 168–173.
[17] C. Maretto, R. Krishna, Catal. Today 52 (1999) 279–289.
[18] J.J. Marano, G.D. Holder, Ind. Eng. Chem. Res. 36 (1997) 2399–2408.
[19] J.J. Marano, G.D. Holder, Fluid Phase Equilib. 138 (1997) 1–21.
[20] Y.N. Wang, Y.Y. Xu, H.W. Xiang, Y.W. Li, B.J. Zhang, Ind. Eng. Chem. Res. 40 (2001) 4324–4335.
[21] R.C. Reid, J.M. Prausnitz, B.E. Poling, The Properties of Gases and Liquids, 4th ed., McGraw-Hill, New York, 1987.
[22] www.athenavisual.com.